Journal of Visualization, Vol. 8, No. 1 (2005)57-64

Effect of the Number of Grooves on Flow Characteristics around a Circular Cylinder with Triangular Grooves

Yamagishi, Y.*[1] and Oki, M.*[2]

*1 Department of Mechanical Engineering, Kanagawa Institute of Technology, 1030 Shimoogino, Atugi-shi, Kanagawa 243-0292, Japan. E-mail: yamagisi@me.kanagawa-it.ac.jp
*2 School of High-Technology for Human Welfare, Tokai University, 317 Nishino, Numazu-shi, Shizuoka 410-0395, Japan.

Received 18 May 2004
Revised 12 October 2004

Abstract : In the flow around a circular cylinder, a sudden decrease in the mean drag coefficient occurs at a high Reynolds number, but the same phenomenon occurs at a lower Reynolds number in the case where there exist grooves or roughness on the cylinder surface. In this paper, in order to make clear the flow characteristics around a cylinder with 20, 26 and 32 triangular grooves, the mean drag coefficient, pressure distribution, velocity distribution and turbulence intensity distribution were measured. Moreover, the flow around the cylinder was analyzed by applying the RNG k - ε turbulent model, and the surface flow pattern was investigated using the oil-film technique. From these results, it was found that a sudden decrease in the mean drag coefficient of a cylinder with 32 triangular grooves occurs at a lower Reynolds number compared with 20 and 26 triangular grooves.

Keywords : Circular Cylinder with Grooves, Flow Characteristics, Drag Coefficient, Flow Visualization, Numerical Analysis.

1. Introduction

In the case of a circular cylinder in uniform flow, a sudden decrease in the mean drag coefficient occurs at a high Reynolds number Re =3x10^5, but it is known that the same phenomenon occurs at a lower Reynolds number in the case where there exist grooves or roughness on the cylinder surface. Such a drag reduction phenomenon can be applied to a vessel, an airplane, an electricity line, etc. for improving energy efficiency, or reducing the wind load. A circular cylinder with roughness was examined experimentally by Achenbach and others (Achenbach, 1971 and Achenbach et al., 1981), Nakamura and others (Nakamura et al., 1982) and Adachi and others (Adachi et al., 1989 and 1995). A cylinder with grooves was examined by Kawamura and others (Kawamura et al., 1984), Oki and others (Oki et al., 1994), Lee and others (Lee et al., 1996) and Kimura and others (Kimura et al., 1991). A flat plate with grooves and a sphere with dimples were examined by Aoki and others (Aoki et al., 2000 and 2003).

We already studied the effect of depth and shape of the grooves (Oki et al., 1999, Yamagishi et al., 2004). However, the effect of the number of grooves on the flow characteristics around a cylinder has not been completely clarified yet. The purpose of this study is to investigate the mechanism underlying the flow of three kinds of cylinders with triangular grooves placed at the different intervals along the cylinder [in the horizontal direction in Fig. 1(a)] by using experiments, numerical

analysis and visualization.

2. Experimental Apparatus and Method

2.1 Experimental apparatus

Figure 1(a) shows the circular cylinder with triangular grooves used for this experiment. The cylinder with grooves is made of aluminum and is 420 mm in length and 48 mm in diameter (d). The triangular grooves of 3.6 mm in width and 0.5 mm in depth (k_s) were carved to the surface of each cylinder at intervals of 18°, 13.85° and 11.25° along the cylinder, the number of grooves were 20, 26 and 32, respectively and the equivalent roughness had a value of k_s/d=10.4x10^{-3}, as shown in Figs. 1 (b), (c) and (d).

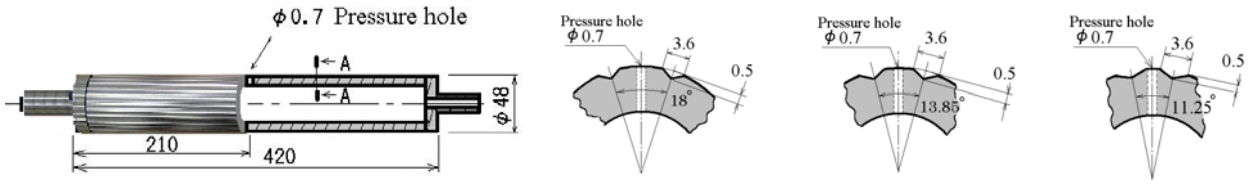

(a) Circular cylinder with triangular grooves (A-A section) (b) 20 grooves (c) 26 grooves (d) 32 grooves

[Unit: mm]

Fig. 1. Shape of grooves and location of the pressure hole.

A schematic diagram of the experimental apparatus is shown in Fig. 2. The experiments were conducted in a wind tunnel of 400 mm x 400 mm cross section. The wind tunnel is a circulating type, with a turbulence intensity of about 0.65% and a maximum speed of around 35 m/s. The cylinder was placed vertically in the measuring section of the wind tunnel and the convex part was set facing the direction of flow. The flow around the cylinder was examined at different Reynolds numbers $Re=Ud/\nu$ (d: diameter of the cylinder, U: uniform flow velocity, ν: kinematic viscosity) ranging from 1x10^4 to 10x10^4.

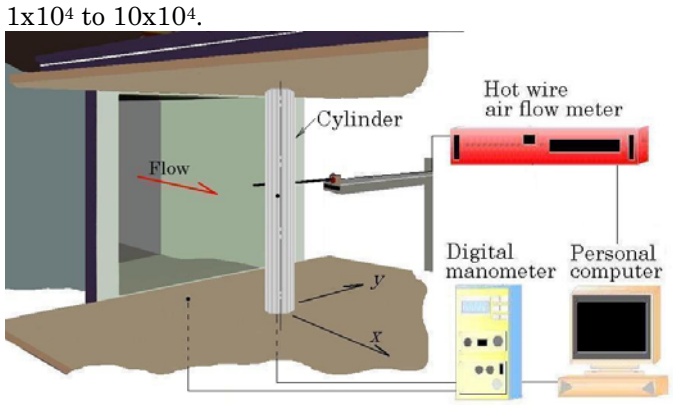

Fig. 2. Experimental apparatus.

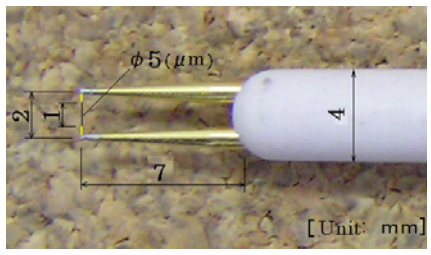

Fig. 3. Prove.

2.2 Measurement and visualization

The drag force is obtained by a wake traverse method based on momentum theory. Measurements of the velocity were made using an IHW hot-wire anemometer (sampling time: 1ms) by moving the hot-wire probe in the direction of the y-axis. Figure 3 shows the prove, KANOMAX Inc.0251R-T5 model used for this experiment. The output signals were digitized on a personal computer. Firstly, the mean drag coefficients C_D of a smooth circular cylinder were obtained using this drag measurement method. Confirming that the value of C_D equal C_D of a smooth cylinder (Nakayama and Boucher, 2000), C_D of the circular cylinder with grooves were obtained.

The difference in pressure between the surface pressure of the cylinder and the static pressure of the tunnel wall was measured using a digital manometer (sampling time: 200ms) and imported into a personal computer.

For visualization, the surface of the cylinder was painted black and covered with a white oil-film that was dissolved in a solution of titanium oxide composed of liquid paraffin and olein-acid. Photographs of the cylinder surface were taken using a digital camera.

The turbulent intensity and velocity were measured by the hot-wire anemometer.

3. Numerical Analysis

Numerical analysis was performed by using the versatile fluid analysis software package Fluent 6.1 using the finite volume method. The analysis was made in unsteady two-dimensional turbulent flow. The turbulent model used the RNG k–ε model with the standard wall function near the surface. A complete view of the mesh and meshes near the circular cylinder surface are shown in Fig. 4. These meshes were chosen as the result of a grid-refinement study (Oki et al., 1999). The boundary conditions are listed in Table 1.

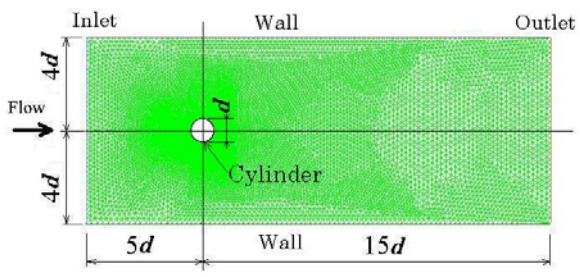

(a) Whole meshes (Grid number ≈ 9x10^4)

Table 1. Boundary conditions

Cylinder surface and wall	u=0, v=0
Inlet	u=U, v=0
	Turbulence intensity=0.65%
Outlet	p_{out}=0

u : Velocity component in the x direction
v : Velocity component in the y direction
U : Uniform flow velocity
p_{out} : Outlet pressure

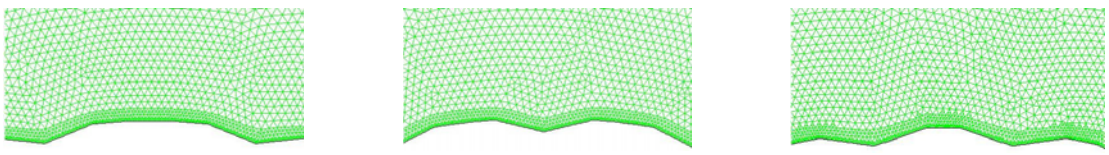

(b) 20 grooves (c) 26 grooves (d) 32 grooves

Fig. 4. Whole meshes and meshes near the circular cylinder surface.

4. Results and Discussion

4.1 Mean drag coefficient

The mean drag coefficient C_D is given from the result of the drag measurements. Figure 5 shows the variations of C_D with the Reynolds number Re for three kinds of circular cylinders with grooves. From this figure, the experimental value of the smooth cylinder and the result of numerical analysis agree well in the range of Reynolds numbers Re =1x10^4 ~ 4x10^5.

Each curve of C_D for the three kinds of circular cylinders with grooves can be divided into subcritical, critical, supercritical and transcritical regions. The value of C_D of each cylinder with grooves is a constant value of about 1.2 in the subcritical region, falls abruptly to a minimum value of about 0.6 at the critical point, and then increases slightly, reaching a constant value of about 0.8 in the transcritical region. The critical point of the cylinder with 20 grooves is about Re =9x10^4, that of the cylinder with 26 grooves is about Re =8x10^4 and that of the cylinder with 32 grooves is about Re =4x10^4. The sudden decrease of C_D occurs at a lower Reynolds number in the case of 32 grooves compared with 20 and 26 grooves. For a wide range of transcritical region, the low value of C_D is nearly constant in the case of 32 grooves. Moreover, the results of the numerical analysis tend to

agree well with the experimental values.

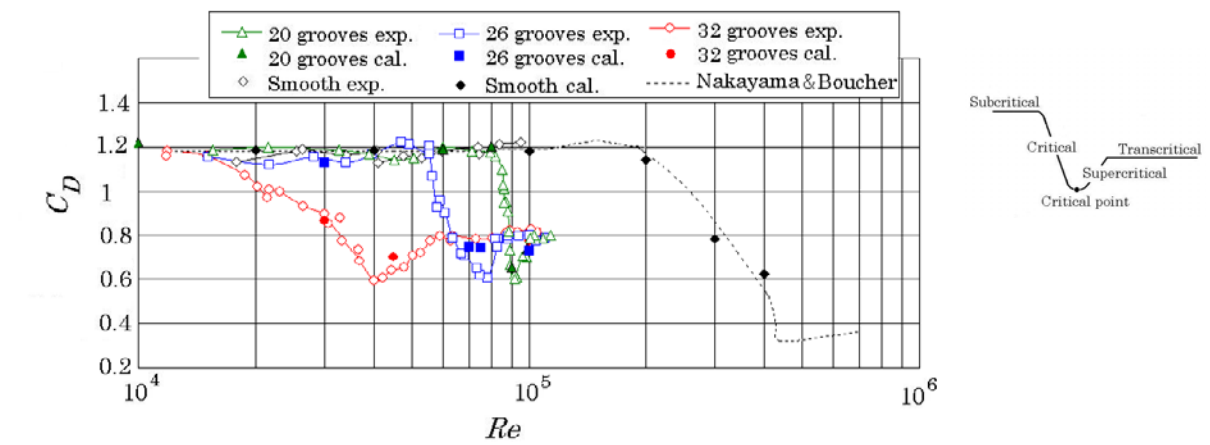

Fig. 5. Mean drag coefficient of circular cylinders with grooves and a smooth cylinder.

4.2 Pressure distribution

The experimental results of the mean pressure coefficient C_p distributions on the circular cylinder surface at Re =4x10⁴ and 8x10⁴ are shown in Figs. 6(a) and (b). The ordinate shows the pressure coefficients C_p and the abscissa shows the angle θ from the stagnation point. The base pressure coefficient C_{pb} for the cylinder with 32 grooves becomes larger compared with the cylinders with 20 and 26 grooves at Re =4x10⁴, and that for the cylinder with 26 grooves becomes larger at Re =8x10⁴. The results experiments have shown that the base pressure coefficient increases near the critical point.

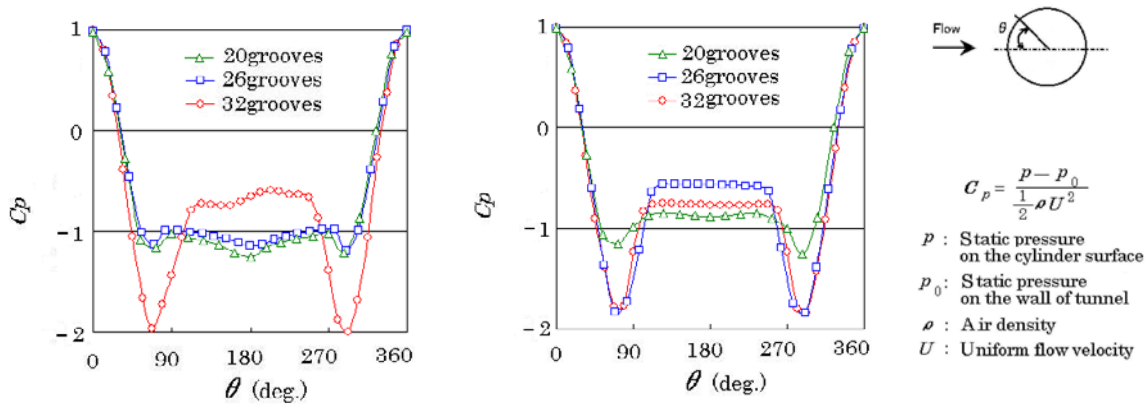

(a) Re =4x10⁴ (b) Re =8x10⁴

Fig. 6. Pressure distribution around the circular cylinder with grooves.

4.3 Separation

Figures 7(a), (b) and (c) show the flow patterns along the circular cylinder surface with three kinds of grooves which were visualized by using the oil-film technique and Fig. 7(d) shows streamlines by numerical analysis with 26 grooves for Re =4x10⁴~10x10⁴. The separation point of the cylinder with grooves shifts to the upstream side in the subcritical region, to the downstream side in the range of the critical point from the subcritical region and to the upstream side in the range of the transcritical region from the critical point. The surface flow patterns obtained by using the oil-film technique and by numerical analysis agree well.

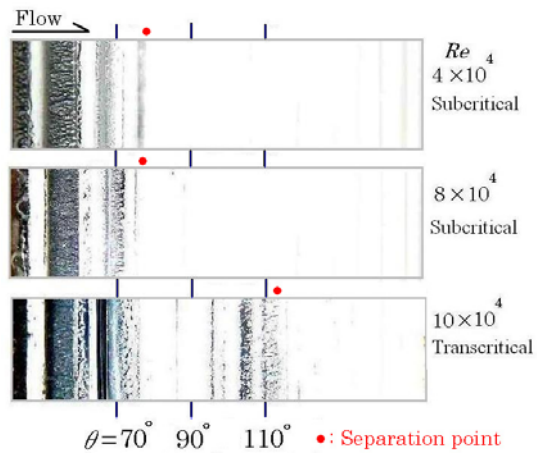

(a) 20 grooves

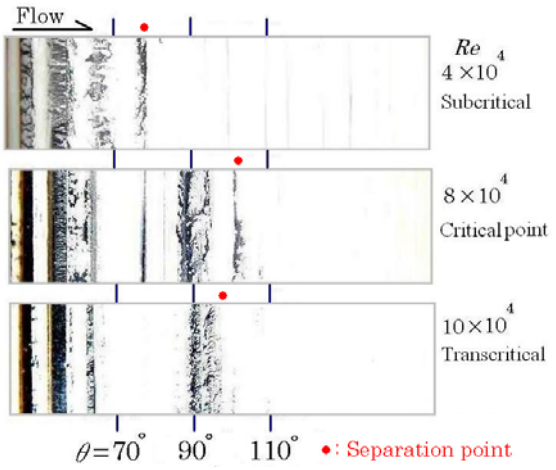

(b) 26 grooves

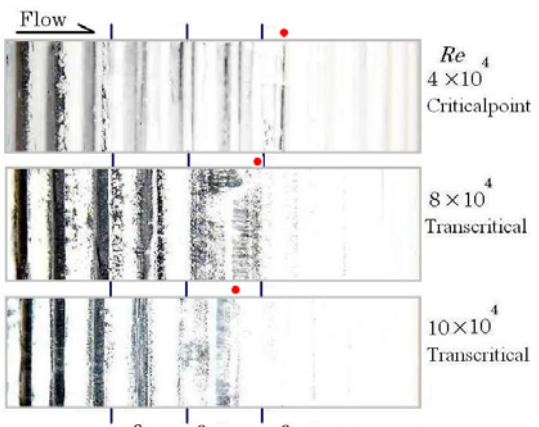

(c) 32 grooves

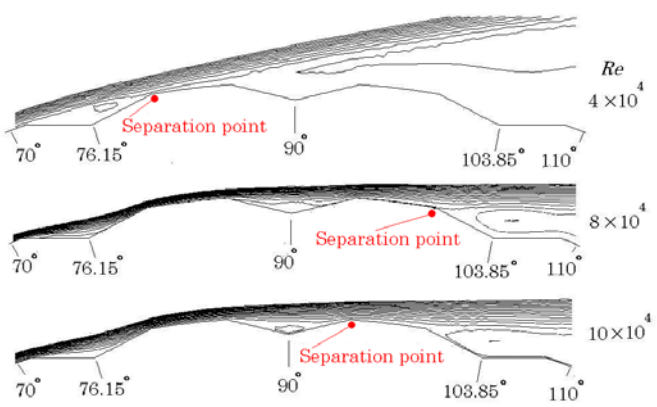

(d) Numerical analysis (26 grooves)

Fig. 7. Oil-pattern and streamlines along the circular cylinder surface with grooves.

4.4 Turbulent kinetic energy distribution

The computational results of the turbulent kinetic energy k distributions behind the circular cylinders with 20 and 26 grooves at Re =8x10^4 are shown in Figs. 8(a) and (b). The cylinder with 20 grooves is in the subcritical flow and that with 26 grooves is in the flow of the critical point. The maximum value of the turbulent kinetic energy behind the cylinder with 20 grooves becomes larger compared with that with 26 grooves.

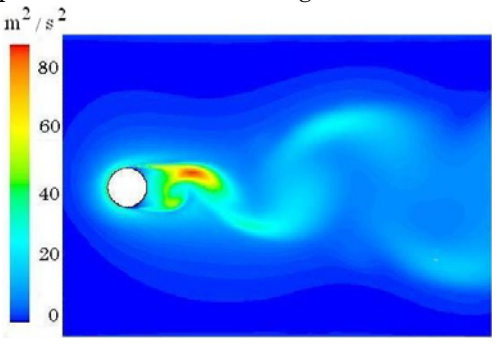

(a) 20 grooves (Subcritical)

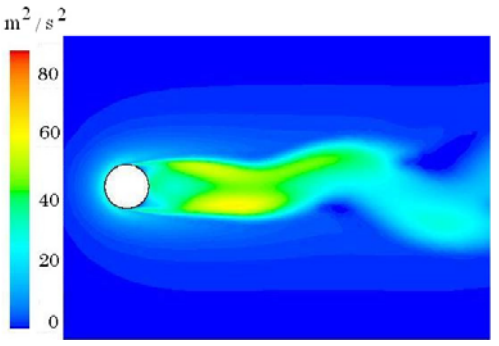

(b) 26 grooves (Critical point)

Fig. 8. The turbulent kinetic energy distribution behind the circular cylinder with grooves (Re =8x10^4).

The experimental results of the turbulence intensity distributions u_t/U (u_t: turbulent velocity component in the x direction) at x/d =1.1 and 2.0 behind the cylinders with 20 and 26 grooves at Re =8x10^4 are shown in Figs. 9(a) and (b), respectively. The trends in the turbulence intensity distribution of Fig. 9 and the turbulent kinetic energy distribution of Fig. 8 are in close agreement. The value of turbulent intensity behind the cylinder with 20 grooves becomes larger compared with that with 26 grooves. The position where the turbulence intensity reaches the maximum value shifts to a low y/d in the case where there exist 26 grooves on the cylinder surface.

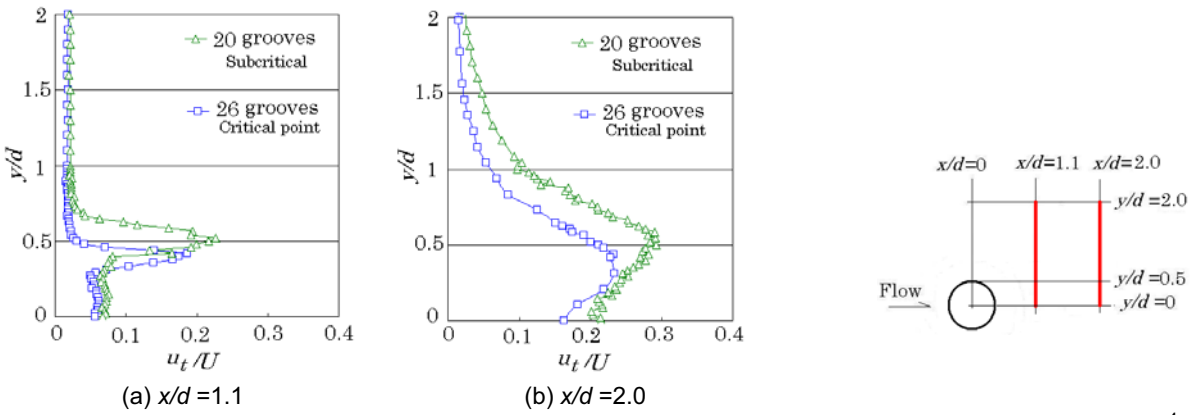

(a) x/d =1.1 (b) x/d =2.0

Fig. 9. The turbulence intensity distribution behind the circular cylinder with grooves (Re =8x10^4).

The turbulent kinetic energy k distributions near the surface of the cylinders with 20 and 26 grooves at Re =8x10^4 are shown in Figs. 10(a) and (b). The turbulent kinetic energy near the surface of the cylinder with 26 grooves becomes larger compared with that with 20 grooves.

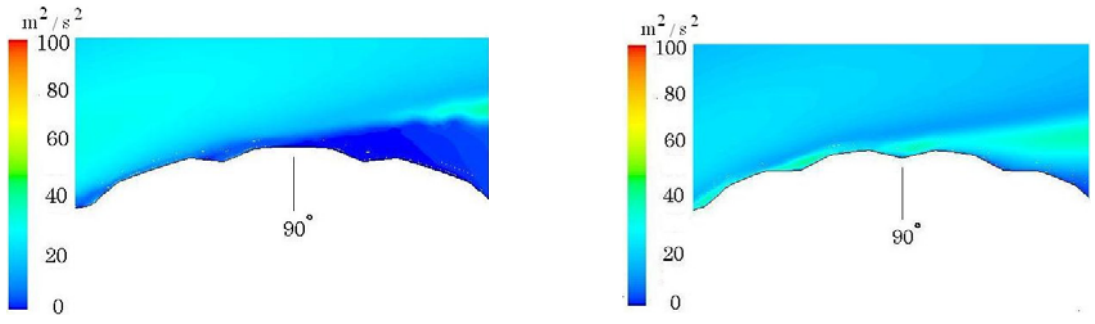

(a) 20 grooves (Subcritical) (b) 26 grooves (Critical point)

Fig. 10. The turbulent kinetic energy distribution around the circular cylinder (Re =8x10^4).

Figures 11(a) and (b) show the velocity distributions at θ=90° near the surface of the cylinders with 20 and 26 grooves, showing experimental results and computational results, respectively, at Re =8x10^4. The results of the numerical analysis tend to agree well with the experimental values. The velocity near the cylinder surface with 26 grooves increases since the turbulent kinetic energy increases in the boundary layer.

The experimental results of the turbulence intensity distribution u_t/U (u_t: turbulent velocity component in the x direction) and the computational results of the turbulent kinetic energy distribution k/U^2 at x/d=1.1 behind the cylinder with 32 grooves at Re =3x10^4 and 10x10^4 are shown in Figs. 12(a) and (b), respectively. The trends in the turbulence intensity distribution and the turbulent kinetic energy distribution are in close agreement. The width of the wake behind the cylinder of the transcritical flow becomes smaller compared with that of the critical flow.

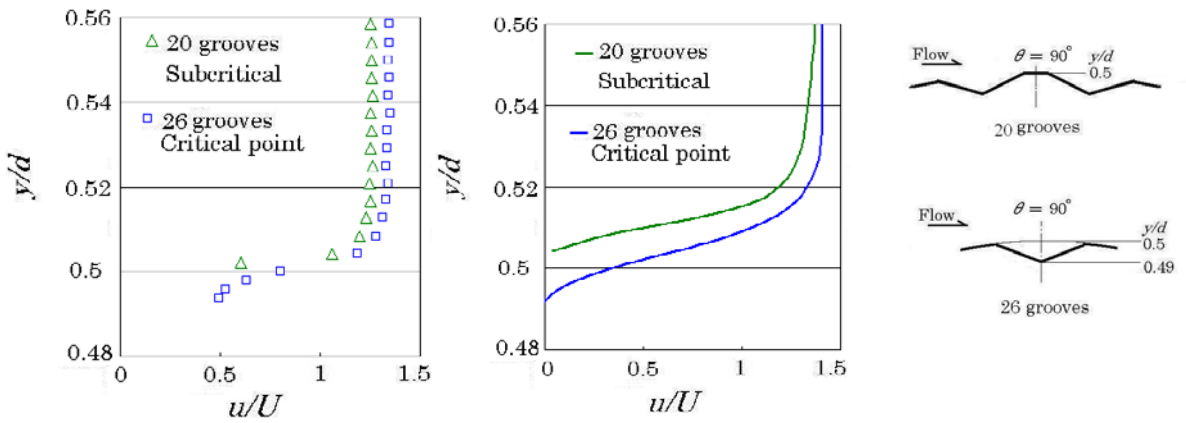

(a) Experimental results (b) Computational results

Fig. 11. Velocity distribution near the surface of the circular cylinder with grooves (θ =90°, Re =8x10^4).

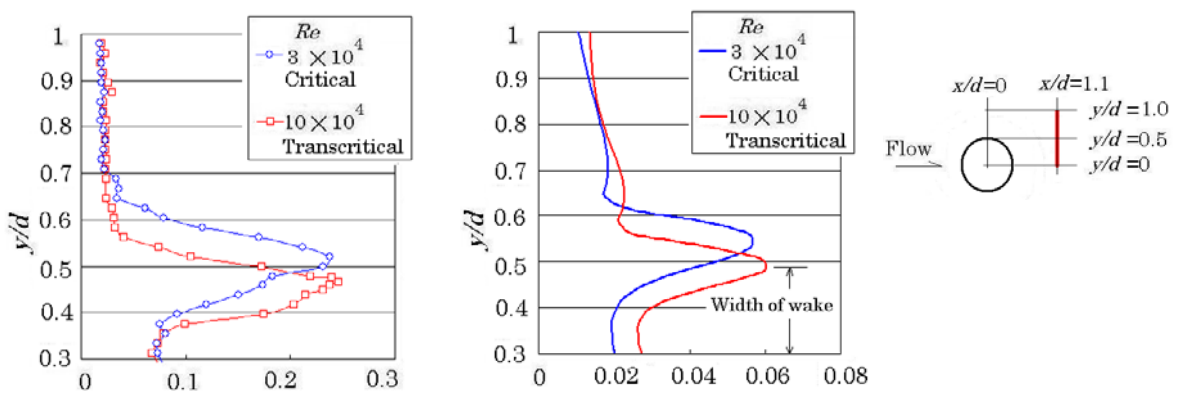

(a) Turbulence intensity distribution (b) Turbulent kinetic energy distribution

Fig. 12. Turbulence intensity and kinetic energy distribution behind the circular cylinder with 32 grooves.

5. Conclusions

The results of experiments and numerical analysis around three kinds of circular cylinders with triangular grooves lead to the following conclusions:

(1) The mean drag coefficients for the cylinder with triangular grooves can be divided into subcritical, critical, supercritical and transcritical regions.

(2) The mean drag coefficient for each cylinder with grooves is a constant value of about 1.2 in the subcritical region, falls abruptly to a minimum value of about 0.6 at the critical point, and then increases slightly, reaching a constant value of about 0.8 in the transcritical region. The sudden decrease in the mean drag coefficient of a cylinder with 32 grooves occurs at a lower Reynolds number compared with 20 and 26 grooves.

(3) The surface flow pattern using the oil-film technique and numerical analysis agree well.

(4) The velocity near the cylinder surface with grooves increases since the turbulent kinetic energy increases in the boundary layer. Therefore, the separation point of the cylinder with grooves shifts to the downstream side and the mean drag coefficient becomes small.

References

Achenbach, E., Influence of surface roughness on the cross-flow around a circular cylinder, Journal of Fluid Mechanics, 46-2 (1971), 321-335.

Achenbach, E. and Heinecke, E., On vortex shedding from smooth and rough cylinders in the range of Reynolds numbers 6x10^3

to 5x10^6, Journal of Fluid Mechanics, 109 (1981), 239-251.
Adachi, T., Ono, H., Matsuuchi, K., Kawai, T. and Cho, T., Flow around a circular cylinder in the High Reynolds Number Range, Transactions of the Japan Society of Mechanical Engineers (in Japanese), 55- 511, B (1989), 685-692.
Adachi, T., Ozaki, T., Yamamoto, T., Eguchi, Y., Matsuuchi, K. and Kawai, T., Study of the Universal Strouhal Number over the Wide Reynolds Number Flow Range (Effect of Surface Roughness), Transactions of the Japan Society of Mechanical Engineers (in Japanese), 61- 583, B (1995), 793-799.
Aoki, K., Okanaga, H. and Nakayama, Y., Control of Boundary Layer on a Flat Plate by Means of Cavity Flow, Journal of Visualization, 3-3 (2000), 211-220.
Aoki, K., Ohike, A., Yamaguchi, K. and Nakayama, Y., Flying Characteristics and Flow Pattern of a Sphere with Dimples, Journal of Visualization, 6-1 (2003), 67-76.
Kimura, T. and Tsutahara, M., Fluid dynamic effects of grooves on circular cylinder surface. AIAA J., 29-12 (1991), 2062-2068.
Kawamura, T. and Kuwahara, K., Computation of High Reynolds Number Flow around a Circular Cylinder with Surface Roughness, AIAA paper, 84-0340 (1984), 1-11.
Lee, S., Aoki, K. and Oki, M., The flow pattern and characteristics around a rotating circular cylinder with grooves, Proc. of the 4th Asian Symp. on Visualization, (Beijing), (1996), 613-618.
Nakamura, Y. and Tomonari, Y., The effects of surface roughness on the flow past circular cylinders at high Reynolds Numbers, Journal of Fluid Mechanics, 123 (1982), 363-378.
Nakayama, Y. and Boucher, R. F., Introduction to Fluid Mechanics (reviesd), (2000), 155, Butterworth- Heinemann, Oxford.
Oki, M., Suehiro, M., Aoki, K. and Nakayama, Y., Effect of grooves' depth on circular cylinder, FLUCOME'94 (Toulouse), (1994), 811-816.
Oki, M., Aoki, K. and Nakayama, Y., Effect of grooves' depth for flow characteristics around a circular cylinder with grooves, Transaction of the Japan Society of Mechanical Engineering (in Japanese), 65-631, B (1999), 870-875.
Yamagishi, Y. and Oki, M., Effect of Groove Shape on Flow Characteristics around a Circular Cylinder with Grooves, J. of Visualization, 7-3 (2004), 209-216.

Author Profile

Yoichi Yamagishi: He received his M.Sc. (Eng.) degree in Mechanical Engineering in 1978 from Tokai University. After obtaining M.Sc. he worked as an engineer at Hibiya Engineering, Ltd. He then became a Research Assistant of Kanagawa Institute of Technology. His current research interests are experimental and computational fluid dynamics.

Makoto Oki: He received his M.Sc. (Eng.) degree in Mechanical Engineering in 1976 from Tokai University and his Ph.D. in Mechanical Engineering in 2000 from the same university. After obtaining M.Sc. he worked as a system engineer at Japan Advanced Numerical Analysis, Inc. He then became an Assistant Professor of Tokai University, and currently is an Associate Professor. His current research interests are computational fluid dynamics, computer graphics and internet application.